

REGIONAL CODA MAGNITUDES IN CENTRAL ASIA AND $m_b(L_g)$ TRANSPORTABILITY

W.S. Phillips, H.J. Patton and H.E. Hartse
Los Alamos National Laboratory

K.M. Mayeda
Lawrence Livermore National Laboratory

Sponsored by the National Nuclear Security Administration
Office of Nonproliferation Research and Engineering
Office of Defense Nuclear Nonproliferation

Contract No. W-7405-ENG-36

ABSTRACT

Local and near regional coda have been shown to provide accurate and precise estimates of source, path and site effects. Using empirical methods, we investigate the use of coda to determine moments and magnitudes using regional distance (to 2500 km) data from 21 stations in central Asia and China. We find source levels for bands between 33 s and 8 Hz from events recorded at Urumchi (WMQ) to be a factor of two more consistent for coda than for direct waves, for bands outside the microseism range. However, the anticipated path averaging of regional coda is insufficient to remove bias in all but the lowest frequency bands. We correct for path bias by spatially interpolating coda levels relative to $m_b(\text{PDE})$. For higher bands (1 Hz), the spatial correction patterns vary by an order of magnitude and are similar to patterns obtained using direct L_g . For the lowest band (20-33 s) the maximum spatial variation shrinks to under a factor of 4 and changes sign, reflecting effects other than crustal Q. Thus, the low frequency coda could be useful for correcting for source effects in empirical or tomographic path studies, which is currently performed using m_b . After removing path bias from coda measurements, we find that amplitude measurement consistency between all 21 stations varies considerably from pair to pair ($\sigma = 0.12$ to 0.37), with longer interstation distance, low-Q surroundings and poor site conditions yielding the least stable measurements. CMT based moments (M_w) derived from 20-33 s WMQ coda are verified by comparing with moments derived from waveform fitting studies ($\sigma = 0.18$).

We continue investigations into the transportability of regional magnitudes using the $m_b(L_g)$ scale devised by Nuttli. Previous work has shown that $m_b(L_g)$ is portable for earthquakes provided that L_g attenuation is well calibrated for propagation paths. In this study, our focus shifts to explosion sources, and the question of transportability of $m_b(L_g)$ for different test sites. We revisit Nuttli's results, which were based on observations at far-regional and teleseismic distances, and depended critically upon accurate knowledge of the $L_g Q_0$. In this paper, measurements of $m_b(L_g)$ are reported for stations within 1000 km, and as such, errors due to uncertainties in the path correction are smaller than was the case for Nuttli's measurements.

KEY WORDS: magnitude, regional monitoring, $m_b(L_g)$, coda

OBJECTIVES

We test the ability of coda methods to reliably estimate moment and magnitude at regional distances in central Asia and China. The methods of Mayeda *et al.* (2000) are extended to account for regional path variation and relative site terms in a multiple station approach. Further, we study the applicability of M_s - m_b discrimination to regional distances through investigations of $m_b(L_g)$ transportability and physical basis.

RESEARCH ACCOMPLISHED

Coda Studies. The stability of coda, with respect to path, has been well documented at local distances. The stability, or uniform coda shape, is consistent with the model of coda as the superposition of waves backscattered from random heterogeneities in the earth's crust and upper mantle (Aki, 1969). Thus, coda reflect path-averaged properties of a given region. The coda stability allows the isolation of relative, radiation-pattern averaged source

effects apart from site and path effects. The numerous independent measurements that can be made in the coda result in a high precision, allowing a single station to yield results comparable to a network average. These techniques were used to estimate absolute source spectra and study source scaling using data from analog, spectral analyzing seismographs (Aki and Chouet, 1975; Chouet *et al.*, 1978; Rautian and Khalturin, 1978; Tsujiura, 1978). In addition, coda duration was found to give stable magnitude estimates (Bisztricsany, 1958) and its use became widespread in local network operations. Furthermore, Aki (1980) proposed the use of coda amplitudes, rather than duration, to obtain higher precision magnitude estimates.

The success of coda methods with dense network, local earthquake data occurs because data in the late, or path-averaged, portion of the coda is generally available. The late coda is loosely defined to begin at twice the S-arrival time (Rautian and Khalturin, 1978), taken from observations of the point at which coda shapes begin to coalesce. This poses a problem for the use of coda at regional distances because less data is available at twice the *S* (or *L_g* or surface wave) arrival, so sufficient path averaging may or may not have occurred to make coda useful for estimating source spectra. However, Mayeda (1993) showed that magnitudes of NTS explosions based on regional *L_g* coda were a factor of 5 more stable than magnitudes based on direct *L_g*. In addition, Hartse *et al.* (1995) demonstrated that spectral ratio discriminants were effective using far local to near regional coda data from NTS explosions and nearby earthquakes. Finally, Mayeda and Walter (1996), showed that a Green's function technique could be used to obtain absolute spectra and study source character using regional coda from western U.S. earthquakes and explosions.

In previous work (Phillips *et al.*, 2000a), we applied the empirical techniques of Mayeda *et al.* (2000) to study regional coda in the 1 Hz band at stations Makanchi (MAK), Kazakhstan, and Urumchi (WMQ) and Lanzhou (LZH), China. While the consistency between coda measurements at MAK and WMQ was found to be a factor of two better than for direct *L_g*, biases were noted in the measurements due to differing propagation paths.

Because we measure the coda close to the *L_g* arrival, we might expect path effects to be present in the results. To examine this, we interpolated distance-corrected 1 Hz coda source factors after subtracting *m_b* (PDE) using kriging (Phillips *et al.*, 2000a; also included in Figure 4). Results show strong laterally varying effects that correlate well with known *L_g* path effects in this region (Phillips, 1999). These effects can be corrected, but the inter-station consistency improves little due to correlated adjustments.

Inter-station consistency is often used to demonstrate the stability of coda amplitude measurements. However, based on the path bias we observe and the lack of improvement in consistency after the bias is corrected for, we conclude that the interstation consistency is not sufficient to demonstrate the accuracy of coda measurements, but can be a good indicator of precision. To demonstrate accuracy, we must, instead, compare coda results with independently derived moment and magnitude results (Mayeda *et al.*, 2000).

In the current study, we apply coda techniques to 13 bands, from 33 s to 8 Hz, and 21 stations in China and central Asia (Figure 1). As before, we follow the method of Mayeda *et al.*, (2000). After smoothing envelopes of bandpassed seismograms, coda decay, *b*, is determined for a suite of records

$$A(t) = A_0 t^{-0.7} \exp -b(\Delta)t,$$

and then expressed as a function of distance, Δ , via a hyperbolic fit. The time origin is placed at the peak envelope, accommodating different phases and group velocities for varying distance and frequency. We then obtain coda source factors (A_0) by re-fitting the coda decay data with the predicted $b(\Delta)$. The coda source factors are further corrected based on a linear fit of $A_0 - m_b$ (PDE) versus distance prior to kriging to obtain regionally varying path corrections. Kriged corrections are obtained using all data except for the measurement being corrected. Absolute spectra are then obtained using a frequency-dependent correction that produces flat low-frequency spectra below the estimated corner frequency in an average sense for a suite of events, followed by a tie to independently determined moments (CMT and/or literature values). Relative site terms are introduced based on common event measurements throughout the network, which avoids interstation discrepancies that result from poor spatial and temporal distributions of calibration events.

We obtain highest precision, in terms of interstation amplitude scatter, in bands near 1 Hz ($\sigma = 0.13$ for MAK-WMQ; Figure 2). Coda provide more consistent measurements than direct phases in nearly all bands, including the

lowest band we examined (20-33 s), with low frequency bands near the microseism range the worst performers in terms of scatter relative to direct phases and the number of measurements that pass signal-to-noise criteria. Examining all pairs of stations, we find that interstation scatter is quite variable. For example, preliminary results show 1 Hz scatter measures 0.12 between Enshi (ENH) and Xian (XAN), and 0.37 between Kunming (KMI) and LZH (Figure 3). Scatter generally increases with interstation distance, reflecting more diverse path effects, which may not have been completely accounted for. Some of the best pairs of stations lie in high-Q regions (1 Hz L_g $Q > 600$ from tomographic imaging; Phillips *et al.*, 2000b). Recall that we have attempted to remove path effects using interpolation (kriging) methods, but this will be most successful for events from areas of high activity. Certain stations, such as LZH, yield higher scatter in many combinations, indicating the influence of site effects such as reverberation, which could contaminate the coda and cause the coda measurements to reflect amplitudes of direct waves more closely.

To validate the accuracy of coda measurements, we must compare with independently derived quantities. After calibrating 20-33 s WMQ coda using CMT moments, we compare to a collection of moments derived from waveform modeling studies, obtaining a scatter of 0.18 (Mw units).

As mentioned above, interpolated (kriged) path correction surfaces for 1 Hz coda are qualitatively similar to those of direct L_g (Figure 4). This results from inadequate path averaging of the scattered waves in the coda, causing coda amplitudes to reflect anelastic properties of the crust over a limited region surrounding the direct path. This holds for nearly all bands; however, at the lowest frequencies, the path corrections become subtle and in the lowest band (20-33 s) the pattern flips sign and is nearly anticorrelated with the 1 Hz pattern (Figure 4). The low frequency pattern cannot reflect crustal attenuation, because it is opposite to what is expected. Instead, it reflects bias in m_b , which will be affected by regionally varying attenuation in the upper mantle, or a Rayleigh wave generation term that systematically varies throughout the region. In either case, the variation is small, indicating a level of stability independent of path that could be taken advantage of in source and path studies in this region.

$m_b(L_g)$ Transportability. A major goal of regional magnitude development is to extend the applicability of M_s - m_b discrimination to smaller events. An ideal regional M_s - m_b discriminant is (1) effective at small magnitudes, (2) transportable to all geological environments, and (3) supported by a sound physical basis. Because L_g amplitudes are often the largest on regional seismograms, this phase offers the best opportunity to monitor small explosions near the detection threshold. Furthermore, O. Nuttli claimed in the 1980's that $m_b(L_g)$ is transportable to all continental areas, a claim that was never tested at the time but was generally accepted by the monitoring community by virtue of its role solving the test-site bias problem. At Los Alamos, we are continuing to develop $m_b(L_g)$ by carrying out studies of its transportability and by building a data base of calibration data for areas of monitoring interest.

It is important to stress that the development of a regional M_s - m_b discriminant represents a major paradigm shift. Instead of basing m_b on the amplitude of a P -wave pulse, as in the classical teleseismic discriminant, we are proposing the use of regional m_b based on mainly S -energy carried by L_g or coda waves. Furthermore, L_g and coda waves are complex wave trains exhibiting random spectral phase, unlike a pure pulse. For these reasons, regional M_s - m_b relationships might scale quite differently from the classical discriminant. This calls for empirical and theoretical studies to investigate scaling behavior at small magnitudes and to develop a physical basis.

For the past few years, we have studied the transportability of $m_b(L_g)$ for earthquakes and explosions. Results of earthquake studies have been presented in numerous papers, and are summarized only briefly here. Nuttli's claim of transportability depends on two factors: (1) accurate corrections for geometrical spreading and region-specific attenuation, and (2) a region-independent calibration constant used to tie the $m_b(L_g)$ scale to $m_b(P)$. The latter was calibrated only once, for central U. S., where it was found that an earthquake with $m_b(P)$ 5.0 produces a hypothetical, 1-Hz L_g amplitude of 110 microns at a reference distance of 10 km. The studies we have carried out have validated this region-independent constant, 110 microns for m_b 5, for crustal earthquakes in eastern North America, western U. S., central Asia, and central Europe (Patton and Schlittenhardt, 2000; Patton, 2001).

Our approach for testing transportability is given in Figure 5. Earthquake source and propagation phenomena are summarized inside the box in Figure 5(a). Outside the box, data analysis steps are shown: the regional wave forms are passed through a World-Wide Standard Seismographic Network response, and 1-Hz L_g waves are then corrected for Airy phase propagation and region-specific attenuation. M_w - $m_b(L_g)$ scaling relationships are developed using

independent estimates of seismic moment M_o , and statistical tests are run to see if the scaling observations in each region are consistent with a single, unifying relationship. This approach is actually more rigorous than need be since Nuttli claimed transportability of the calibration constant only, not that $m_b(L_g)$ should scale similarly too. Nevertheless, a single scaling relationship satisfies the observations for M_w 4.3 to ~6.0 in all regions tested to date. Provided that path calibration data are accurate for each region, these tests validate a region-independent calibration constant. This remarkable result suggests that excitation amplitudes of 1-Hz L_g waves are relatively insensitive to source radiation patterns and the gross physical properties of the continental crust.

It is noteworthy that a better test would have employed source “potency” instead of seismic moment since potency involves only the parameters that scale with source size, namely fault area and slip. To the extent that source region rigidity varies from one earthquake to the next, this is expected to add variance in $M_w:m_b$ observations, but probably not enough to nullify the transportability results, at least for earthquakes located at seismogenic depths in the crust. On the other hand, the issue of potency versus seismic moment is very important for explosions, as discussed below.

Figure 5(b) summarizes the explosion source as it relates to our transportability studies. The assumption is that far-field propagation should be similar for earthquakes and explosions, and the data analysis is identical. We are faced with three candidate parameters with which to test the portability of $m_b(L_g)$ for explosions: source potency, which is simply the reduced displacement potential, Ψ_∞ , seismic moment, and explosive yield, W . In the 1980’s, transportability was considered with respect to (*wrt*) yield to solve the test-site bias problem, and this approach was favorable from the standpoint of yield estimation. However, to put the test “on par” with tests already conducted on earthquakes, Ψ_∞ or M_o should be used.

If we elect to test transportability on equal footing with earthquake tests, the choice between Ψ_∞ and M_o will make a difference in the outcome of test results. This is because the source medium can vary greatly for explosions, and the calculation of M_o introduces another dependence on material properties ($\rho\alpha^2$). Ψ_∞ is the fundamental seismic parameter equal to the long-period level of the explosion source spectrum, and this is the reference that should be employed to test portability of $m_b(L_g)$ for explosions detonated in different source media. Just as the choice of Ψ_∞ or M_o will make a difference in the outcome of test results, so will the choice of W or Ψ_∞ . Significant differences in material strength and coupling for different media precludes the possibility of $m_b(L_g)$ from being transportable *wrt* both W and Ψ_∞ . These issues about testing the portability for explosions are summarized in Figure 5(c).

Figure 6 illustrates the dependence of scaling relationships based on Ψ_∞ and M_o for explosions in hardrock environments versus explosions at the Nevada Test Site (NTS). $M_w:m_b(L_g)$ relationships compare favorably for the two testing environments, and might suggest transportability for explosions, as this was the basis for such conclusions for earthquakes. $\Psi_\infty:m_b(L_g)$ relationships lead to quite the opposite conclusion. The method used to derive $\Psi_\infty:m_b(L_g)$ relationships is explained in the figure caption. The $\Psi_\infty:m_b(L_g)$ relationship for NTS explosions was confirmed using cavity radius information (see caption).

Comparisons between $\Psi_\infty:m_b(L_g)$ relationships suggest that, for the same long-period level of the source spectrum, 1-Hz L_g waves from hardrock explosions are over a factor of 3 larger than L_g waves from NTS explosions. This result is counter-intuitive since the excitation of P - and S -waves is larger in weaker, more compliant materials. Thus, elastic theory would predict that amplitudes should be larger for NTS explosions. Explosion source phenomenology (Figure 5(b)) is complex, and spectral differences or secondary sources might be significant enough to explain this anomaly. However, for a number of reasons not discussed here because of length restrictions, we believe that effects of spectrum and secondary sources are probably insufficient to offset effects of elastic excitation and account for an additional factor of 3 in amplitude.

CONCLUSIONS AND RECOMMENDATIONS

Coda estimates show up to a factor of 2 improvement in inter-station consistency relative to direct L_g , for most bands (33 s to 8 Hz) and are best for closely spaced central Asia and Chinese stations located in areas of high crustal Q . The interstation consistency reflects the precision of the coda measurement, but not necessarily its accuracy. Accuracy is verified by comparing with independently determined moments; we obtain a scatter of 0.18 (M_w) for moments from low frequency coda at station WMQ. For purposes of calibration, additional independently derived moments for low magnitude events are critical to the success of the coda method.

Studies of $M_w:m_b(L_g)$ scaling relationships for regions around the world have validated the transportability of $m_b(L_g)$ for earthquakes. For explosions, we are faced with testing portability *wrt* yield or *wrt* Ψ_∞ . Using measurements of $m_b(L_g)$ reported by Nuttli for explosions in hardrock environments, the $\Psi_\infty:m_b(L_g)$ relationship is anomalous compared to the relationship for NTS. The problem could be with Nuttli's measurements since they were taken on old analog data for stations at teleseismic distances, and for such long distances, path calibration data had to be known very accurately. We are continuing our investigations of explosion transportability with regional data for stations much closer to the explosion source and with better calibration data.

REFERENCES

- Aki, K. (1969), Analysis of the seismic coda of local earthquakes as scattered waves, *J. Geophys. Res.*, **74**, 615-631.
- Aki, K., (1980), Physical basis of the duration magnitude and recommended practice for coda magnitude determination, *Proc. 17th Ass. ESC, Budapest*, 73-77.
- Aki, K., M. Bouchon and P. Reasonberg (1974), Seismic source function for an underground nuclear explosion, *Bull. Seism. Soc. Am.*, **64**, 131-148.
- Aki, K. and B. Chouet (1975), Origin of coda waves: Source, attenuation and scattering effects, *J. Geophys. Res.*, **80**, 3322-3342.
- Bisztricsany, E.A. (1958), A new method for the determination of the magnitude of earthquakes, *Geofiz. Kozlem.*, **7**, 2.
- Chouet, B., K. Aki and M. Tsujirua (1978), Regional variation of the scaling law of earthquake source spectra, *Bull. Seism. Soc. Am.*, **68**, 59-79.
- Hartse, H.E., W.S. Phillips, M.C. Fehler and L.S. House (1995), Single-station spectral discrimination using coda waves, *Bull. Seism. Soc. Am.*, **85**, 1464-1474.
- Mayeda, K. (1993), MbLgcoda: A stable single station estimator of magnitude, *Bull. Seism. Soc. Am.*, **83**, 851-861.
- Mayeda, K., A. Hofstetter, W.R. Walter and A. Rodgers (2000), Stable source estimates using regional narrow band coda envelopes: Application to CTBT monitoring and seismic hazard prediction in the Middle East region, *Seism. Res. Lett.*, **71**, 209-210.
- Mayeda, K. and W.R. Walter (1996), Moment, energy, stress drop and source spectra of western United States earthquakes from regional coda envelopes, *J. Geophys. Res.*, **101**, 11195-11208.
- Phillips, W.S. (1999), Empirical path corrections for regional phase amplitudes, *Bull. Seism. Soc. Am.*, **89**, 384-393.
- Phillips, W.S., H.E. Hartse and K.M. Mayeda (2000a). Regional coda magnitudes in central Asia, *22nd Seismic Research Symposium*, New Orleans, 107-113.
- Phillips, W.S., H.E. Hartse, S.R. Taylor and G.E. Randall (2000b). 1 Hz Lg Q tomography in central Asia, *Geophys. Res. Lett.*, **27**, 3425-3428.
- Patton, H.J. and J. Schlittenhardt (2000). Network measurements of Nuttli's $m_b(L_g)$ in central Europe: Tests of regional transportability and comparisons with teleseismic m_b . *EOS Trans. AGU*, **81**, F845, (also LAUR-00-4163).
- Patton, H.J. (2001). Regional magnitude scaling, transportability and $M_s:m_b$ discrimination at small magnitudes, *Pure Appl. Geophys., Special Volume on Monitoring a Comprehensive Nuclear-Test-Ban Treaty*, **in press** (also LAUR-99-6705).
- Rautian, T.G. and V.I. Khalturin (1978), The use of the coda for determination of the earthquake source spectrum, *Bull. Seism. Soc. Am.*, **68**, 923-948.
- Tsujiura, M. (1978), Spectral analysis of the coda waves from local earthquakes, *Bull. Earth. Res. Inst., U. Tokyo*, **53**, 1-48.

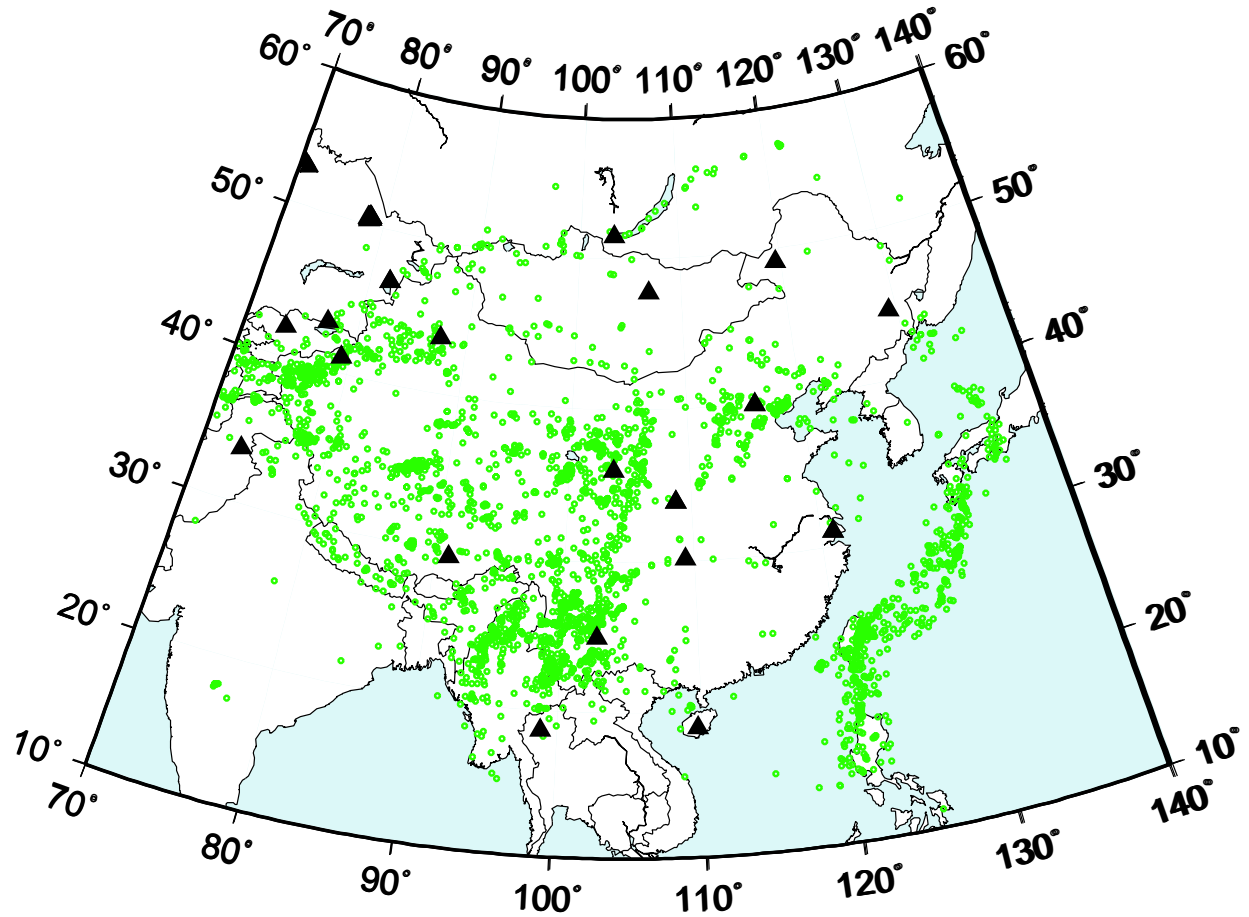


Figure 1. 21 Stations (triangles) and 7400 events (dots) used in the coda study. This data set yielded over 14,000 records, or approximately two per event on average.

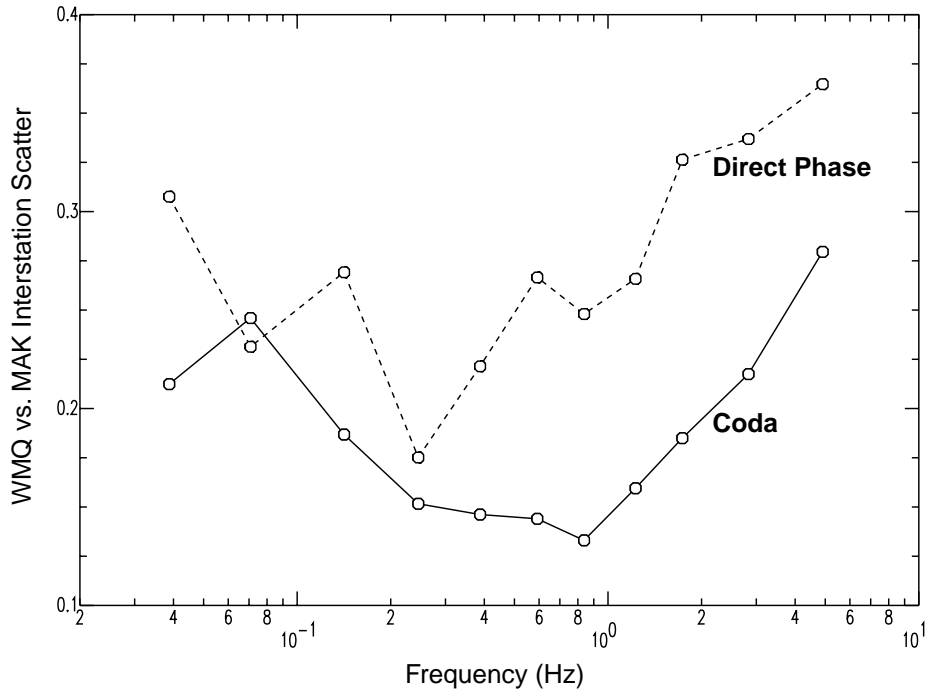


Figure 2. Interstation amplitude scatter for coda (solid line) and direct phases (S , L_g , surface waves; dashed line). Scatter is quantified by the standard deviation of differences between measurements made for common events at stations MAK and WMQ.

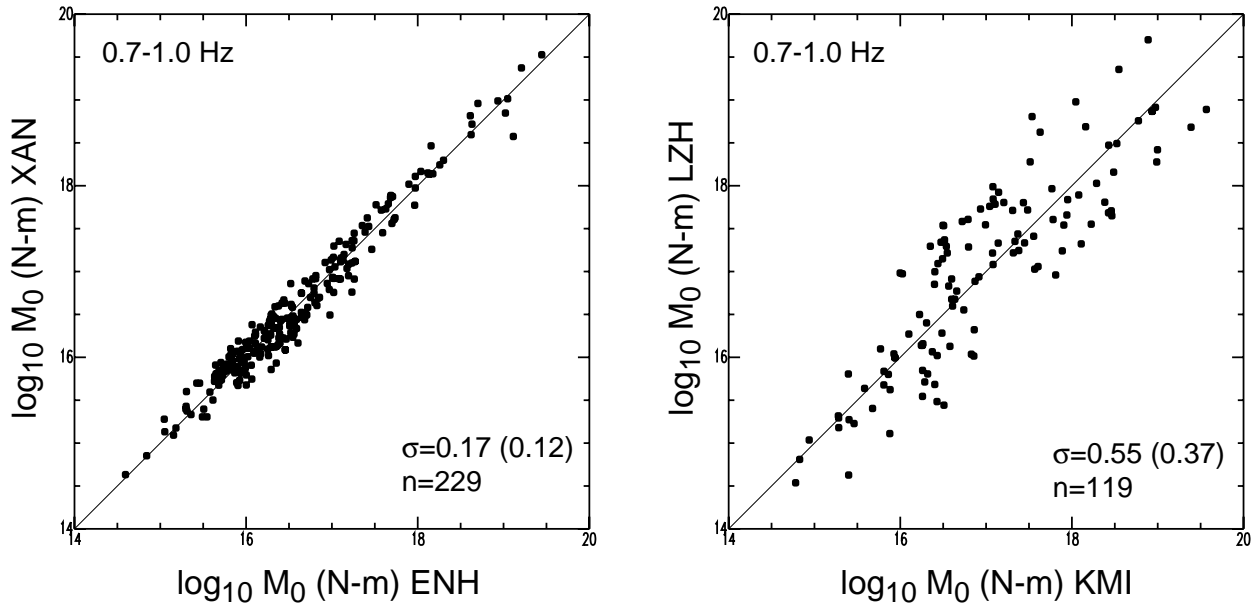


Figure 3. Consistency of coda amplitude measurements between stations ENH and XAN (left) and stations KMI and LZH (right), representing best and worst case pairs in our data set, respectively. These measurements are for the 0.7-1.0 Hz band, and amplitudes have been converted to moment estimates using scaling formulae based on m_b before calibration via CMT estimates. Scatter (see Figure 2 caption) is noted for log M_0 and M_w (in parenthesis) quantities, along with the number of common events.

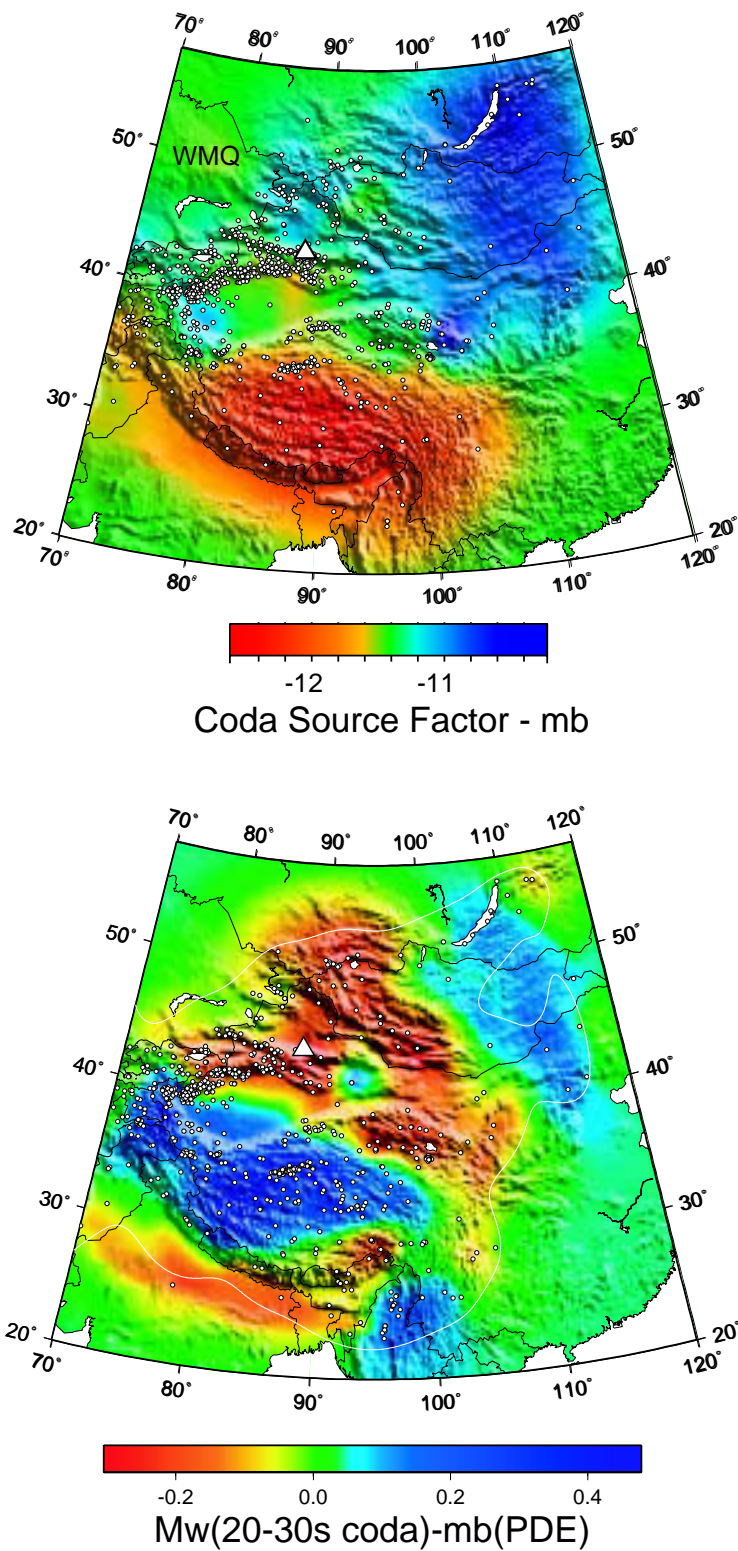
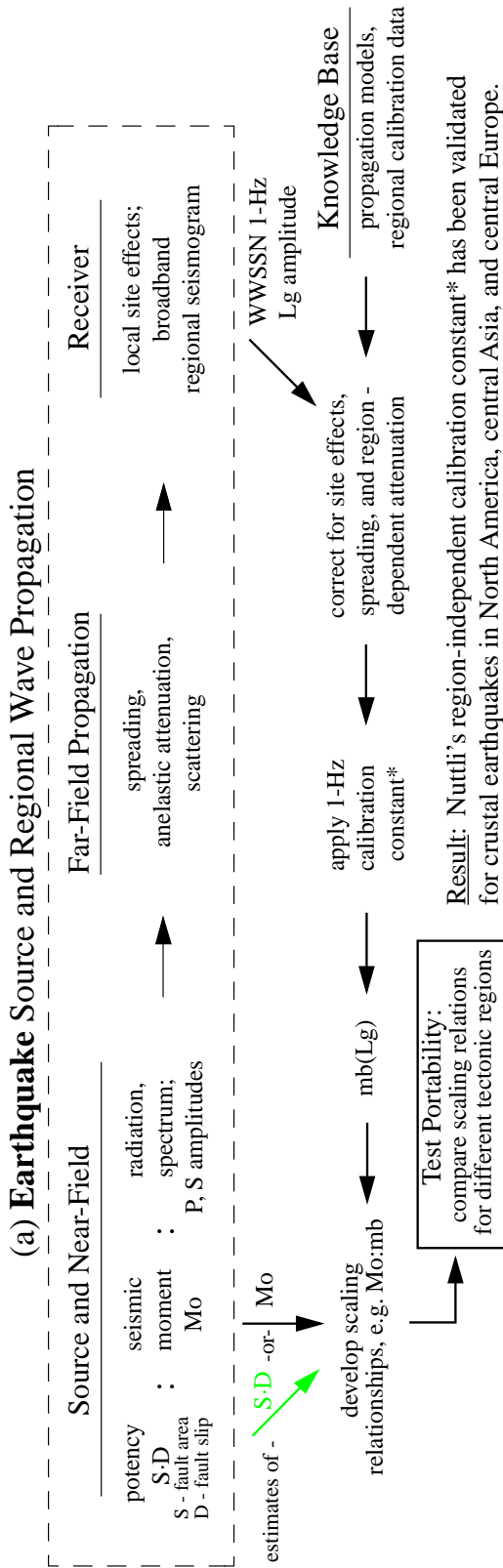


Figure 4. WMQ Coda amplitude (0.7-1.0 Hz; top) and coda Mw (20-33s; bottom) relative to m_b (PDE) obtained by kriging. Color bars represent different scales. Station WMQ is represented by a triangle, and events are represented by small dots.

Testing Portability of $mb(Lg)$ –



(b) Explosion Source Phenomena and Propagation (same as above)

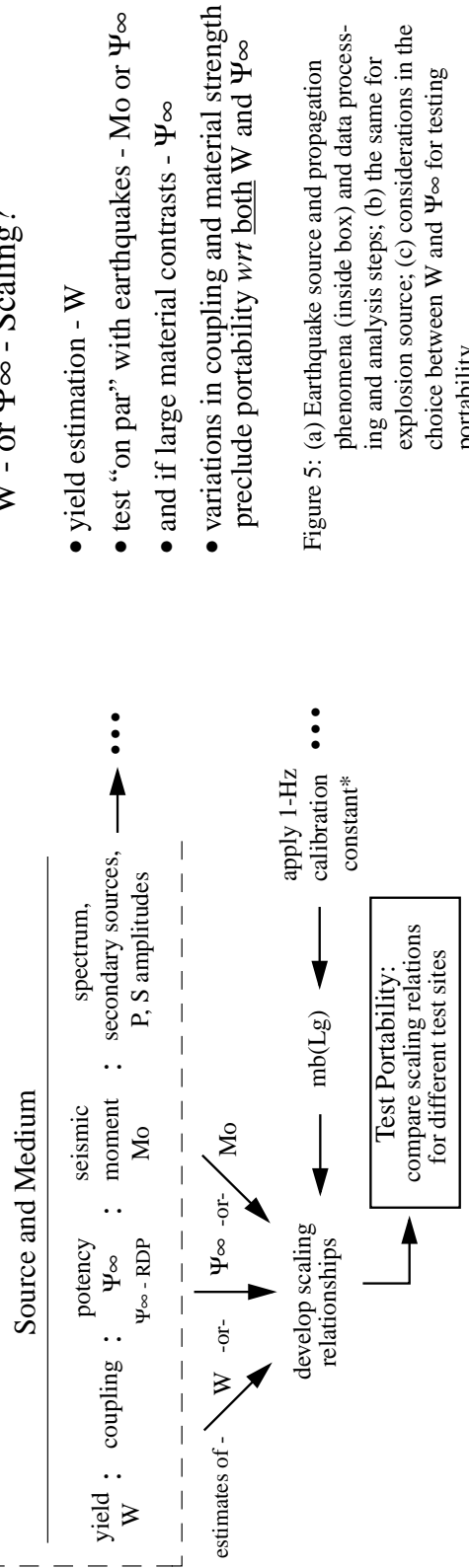


Figure 5: (a) Earthquake source and propagation phenomena (inside box) and data processing and analysis steps; (b) the same for explosion source; (c) considerations in the choice between W and Ψ_{∞} for testing portability

Explosion $m_b(Lg)$ Scaling Relationships: Moment Magnitude M_w and Potency Ψ_∞

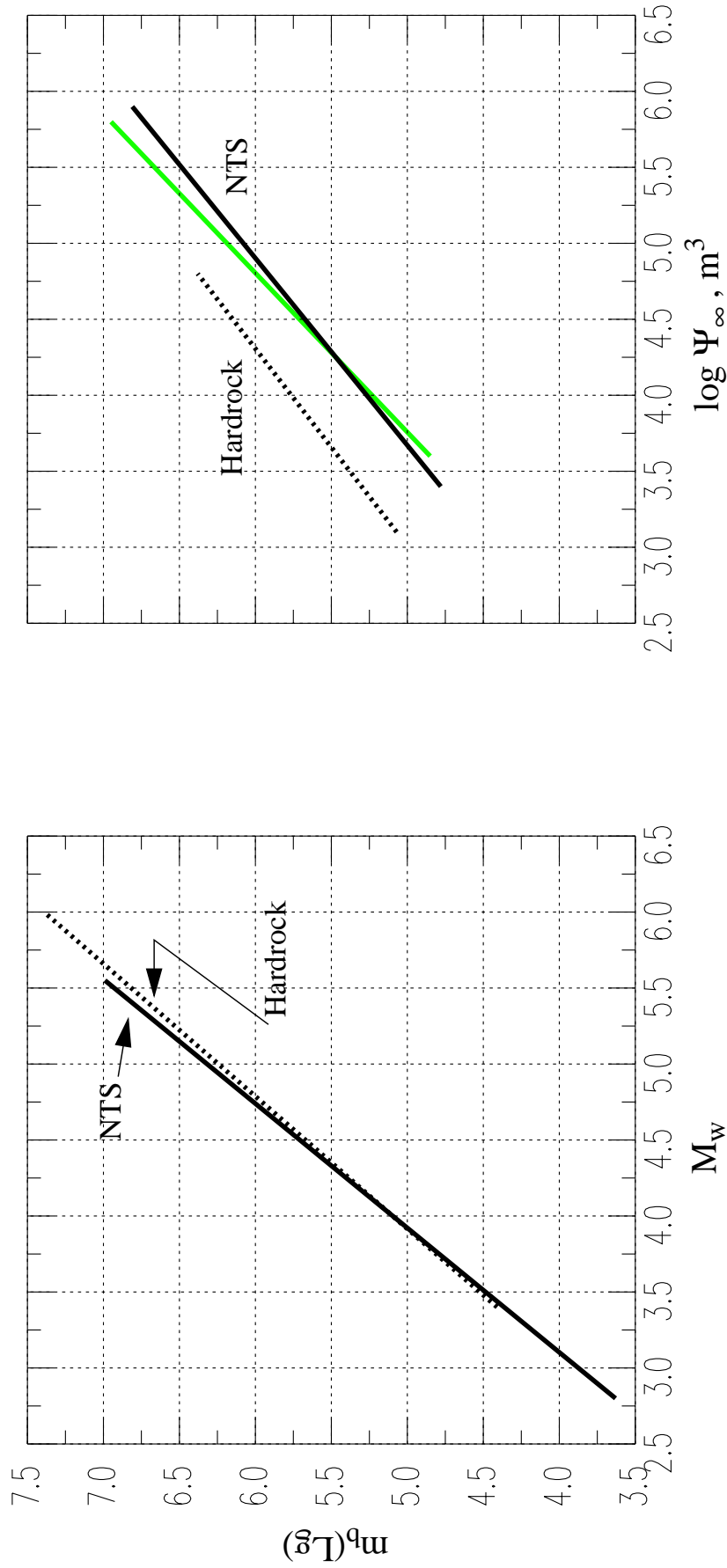


Figure 6: On the left, $M_w : m_b(Lg)$ scaling relationships for NTS and hardrock environments (after Patton, 2001); on the right, $\log \Psi_\infty$ (potency) scaling relationships. Potency scaling for hardrock was derived using the $M_w : m_b(Lg)$ relation and Aki et al.'s (1974) formula, $M_0 = 4\pi\rho\alpha^2\Psi_\infty$, where $\rho = 2500 \text{ kg/m}^3$ and $\alpha = 5000 \text{ m/s}$. For NTS, the black line was obtained by the same method where $\rho = 2000 \text{ kg/m}^3$ and $\alpha = 2700 \text{ m/s}$. The relationship shown as grey line is for shots below the water table and was obtained from a regression of $m_b(Lg)$ versus $1/3 \cdot r_c^3$, where r_c is measured cavity radius in m. Values of $m_b(Lg)$ for hardrock explosions were measured by O. Nuttli.